

Untargeted Metabolomic Analysis of *Randia echinocarpa* Cell Cultures Treated with L-Tyrosine.

Miguel Aguilar-Camacho

Tecnológico de Monterrey: Tecnológico de Monterrey

Carlos E. Gómez-Sánchez

Tecnológico de Monterrey: Tecnológico de Monterrey

Abraham Cruz-Mendivil

Instituto Politecnico Nacional

Diego A Luna-Vital

Tecnológico de Monterrey

José A Guerrero-Analco

Institute of Ecology: Instituto de Ecología

Juan L. Monribot-Villanueva

Instituto de Ecología

Janet Gutiérrez-Urbe (✉ jagu@tec.mx)


Tecnológico de Monterrey <https://orcid.org/0000-0003-1056-7126>

Research Article

Keywords: *Randia echinocarpa*, tyrosine, metabolomics, α -amylase, α -glucosidase, cell suspension culture

Posted Date: January 19th, 2024

DOI: <https://doi.org/10.21203/rs.3.rs-3765446/v1>

License:  This work is licensed under a Creative Commons Attribution 4.0 International License. [Read Full License](#)

Abstract

The addition of precursors, like tyrosine (Tyr), can increase the biomass and specialized metabolites production in plant cell suspensions. There is a need of natural compounds with inhibitory activity against α -amylase and α -glucosidase to decrease the intestinal absorption of simple carbohydrates. It has been previously reported that soluble melanins from the *Randia echinocarpa* fruit inhibit the enzymatic activity of α -glucosidase. Thus, the objective of this study was to analyze the metabolomic profiles of *R. echinocarpa* cell suspensions when treated with different concentrations of Tyr and to assess the inhibitory activities of the cell extracts against α -amylase and α -glucosidase. Methanolic extracts (1 mg/mL) of *R. echinocarpa* cell suspensions inhibited the activity of α -amylase similarly to acarbose at 50 μ M. Nevertheless, no inhibition of α -glucosidase by the extracts was observed. Further purification of the methanolic extracts is required to prevent antagonist effects of the compounds. Four specific chemical profiles were determined by Hierarchical Cluster and Principal Components Analysis. Galactose metabolism and starch/sucrose metabolism were among the main modulated metabolic pathways. Molecular docking showed that compounds Tyr_100 and 200 treatments had an estimated free binding energy of -2.4 to -5.6 kcal/mol and can interact with key amino acids involve with the catalytic activity of α -amylase. The addition of Tyr to the cell suspensions of *R. echinocarpa* can be used to produce α -amylase inhibitory extracts.

INTRODUCTION

The genus *Randia* L. belongs to the Gardenia tribe of the Rubiaceae family, and it is native to America. It comprises 106 species, 62 of them native to Mexico (Villaseñor, 2016). Among these species, *Randia echinocarpa* Sessé et Mociño, known as “papache” in northwestern Mexico, is used in traditional Mexican medicine (Cortés, 2000; Santos-Cervantes et al., 2007). Beneficial biological effects include antioxidant and antimutagenic activities (Santos-Cervantes et al., 2007; Cano-Campos et al., 2011; Montes-Avila et al., 2018). In addition, Cuevas-Juárez et al. (2014) reported that melanins from *R. echinocarpa* exhibited greater α -glucosidase inhibition than acarbose, a well-known drug inhibitor.

The enzymes α -amylase and α -glucosidase are involved in the breakdown of starch and oligosaccharides to glucose, which is absorbed in the small intestine, thus inhibiting these enzymes help to prevent postprandial hyperglycemic peaks (Maidadi et al., 2022). Numerous medicinal plant extracts have been reported to possess potent α -glucosidase and α -amylase inhibitory activity. A wide range of metabolites have been isolated from these plants, including flavonoids, terpenoids, polysaccharides, phenolic acids, alkaloids, and fatty acid derivatives (Kashtoh & Baek, 2023). Therefore, *R. echinocarpa* represents a source of natural compounds with the ability to reduce postprandial blood glucose levels by partially inhibiting carbohydrate-hydrolyzing enzymes such as α -amylase and α -glucosidase.

The accumulation of bioactive compounds in calli and cell suspensions of *R. echinocarpa* under standard culture conditions has been previously demonstrated (Valenzuela-Atondo et al., 2020; Aguilar-Camacho et al., 2023). Different strategies have been utilized to increase the production of plant metabolites including culture media optimization, elicitation, cell immobilization, and precursor feeding (Isah et al., 2017).

Regarding the utilization of metabolic substrates, amino acids are precursors for numerous specialized components of plant cells, such as flavonoids, phenolic acids, coumarins, alkaloids, among others (Feduraev et al., 2020). Tyrosine (Tyr) serves as a precursor for several families of secondary metabolites, including tocochromanols, plastoquinones, isoquinoline alkaloids, several non-protein amino acids, and some phenylpropanoids (Schenck & Maeda, 2018). Tyr increased biomass and secondary metabolite accumulation *in vitro*, as evidenced by enhanced berberine production in *Tinosfera cordifolia* cell cultures (Pillai & Siril, 2022) and increased antioxidant activity in *Cannabis sativa* L. cell cultures (Gabotti et al., 2019). Thus, the exogenous application of precursors at crucial biosynthetic steps could result in enhanced gene expression, enzymatic activities and in consequence, the accumulation of specialized metabolites under *in vitro* conditions (Biswas et al., 2020).

The emergence of omic sciences such as metabolomics opens a new avenue for the understanding of plant metabolites biosynthesis (Jacobowitz & Weng, 2020). The term spectrometric feature, rather than compound, is appropriate because features can include the parental ions of true metabolites and in-source-generated daughter ions (fragments) or adducts (Simpson et al., 2021). Particularly, untargeted metabolomics is based on the comparison of patterns from global chemical profiles obtained from different biological samples, using univariate and multivariate statistical tools (Gómez-Tah et al., 2023).

The information regarding the biochemical composition of *R. echinocarpa* cell cultures is limited. To our knowledge, there are no studies reporting the effects of precursors feeding in the metabolites profile of *R. echinocarpa* cell cultures. This study investigates the metabolic pathways modulated when cell cultures of *R. echinocarpa* are treated with different concentrations of Tyr as precursor. To accomplish our objective, we used an untargeted metabolomic approach by ultra-high performance liquid chromatography coupled to a quadrupole time-of-flight mass spectrometry with electrospray ionization source (UPLC-ESI-QTOF-MS) to identify the metabolic pathways and metabolites significantly affected by Tyr feeding in *R. echinocarpa* cell culture.

MATERIALS AND METHODS

Cell suspensions maintenance

Cell suspensions of *R. echinocarpa* were established as previously described by Aguilar-Camacho et al. (2023). Cells were maintained in the darkness at 25 °C and 120 rpm in an orbital incubator (LabTech, LSI-3016A, Indonesia). Subcultures were performed every 2 weeks (wk), using 2 g of fresh cell biomass as inoculum into 20 mL of fresh Murashige & Skoog (1962) liquid medium containing myo-inositol (100 mg/L), sucrose (30 g/L), 1-naphthalene acetic acid (NAA; 2 mg/L; Sigma-Aldrich, St. Louis, MO, USA) and 6-benzylaminopurine (BAP; 1 mg/L; Caisson Labs, Smithfield, UT, USA).

Preparation of precursors

To increase the production of bioactive secondary metabolites, Tyr was used as precursor. Tyr (Reagent grade, ≥ 98%, Sigma-Aldrich, St Louis, MO, USA) was partially dissolved in 1 mL of HCl (1 N) and further

diluted with distilled water. The solution was sterilized by filtration using a 0.22 µm nylon membrane (Merck Millipore, Tullagreen, Carrigtwohill, Ireland).

Precursor feeding and cell harvesting

The cell suspensions of *R. echinocarpa* were treated with different concentrations of Tyr (0, 50, 100, and 200 mg/L). Precursor concentrations were selected based on previous reports in plant cell suspensions (Gabotti et al., 2019; Balažová et al., 2020; Hegazi et al., 2020). The addition of the different concentrations of Tyr was done at the beginning of the culture period. Cells were harvested at day 16, filtered using a Whatman paper No.1, lyophilized at -50°C for 24 to 48 h (Labconco, Kansas City, MO, USA), and stored at -70°C for further analysis. All the experiments were conducted in triplicates.

Extraction of bioactive compounds

The extraction was carried out according to Juárez-Trujillo et al. (2018). Lyophilized tissue (0.1 g) was homogenized in 2 mL of methanol (99%, HPLC grade) and sonicated 4 cycles for 10 min at 40 kHz (Cole-Parmer 08895-91, Vernon Hills, IL, USA). After sonication, samples were centrifuged (3,500 rpm, 4°C, 15 min) and supernatants were recovered, filtered (Phenomenex, 0.2 µm), and collected in glass vessels. Supernatants were evaporated to dryness under vacuum rotary evaporation (Büchi R11, Büchi, Switzerland) at 42°C. Dried extracts (30 mg) were resuspended in methanol (1 mL) with 0.1% formic acid (both MS grade, Sigma-Aldrich, St. Louis, MO, USA).

α-amylase inhibitory activity

The α-amylase activity assay was adapted from Chandrasekaran et al. (2020). Methanolic extracts were adjusted to 1 mg/mL using 0.02 M sodium phosphate buffer, pH 6.9. Acarbose at 25–150 µM was used as a positive control and 0.5 mL of this solution, buffer (negative control) or samples were added to test tubes with 0.5 mL of α-amylase (13 U/mL, type VI-B from porcine pancreas in phosphate buffer), and incubated at 25°C for 10 min. Then, 0.5 mL of starch (1%, w/v) previously dissolved in the phosphate buffer were added and the mixture reaction was incubated for 10 min. Afterward, 1 mL of dinitrosalicylic acid (DNS) was added to the mixture and the tubes were placed in a water bath at 100°C for 5 min and immediately cooled at room temperature. The reaction mixture was diluted with distilled water (1:10), 0.2 mL of the diluted reaction mixture were placed in a 96-well plate, and the absorbance was read at 540 nm. Results were presented as percent of inhibition as average of three replicates ± standard deviation (SD).

$$Inhibition (\%) = 100 \left(\frac{A_{540} NegControl - A_{540} Sample}{A_{540} NegControl} \right)$$

α-glucosidase inhibitory activity

The protocol by Mojica et al. (2016) was used for the α-glucosidase activity assay. In a 96-well plate, 50 µL of the methanolic extracts (1 mg/mL), or acarbose (positive control) was added to 100 µL of α-glucosidase (1 U/mL, in 0.1 M sodium phosphate buffer, pH 6.9) and incubated for 10 min. A 50 µL aliquot of a 5 mM

p-nitrophenyl- α -D-glucopyranoside solution (in 0.1 M sodium phosphate buffer, pH 6.9) was added to each well and incubated at 25°C for 5 min before reading the absorbance at 405 nm. Results were presented as percent of inhibition.

$$Inhibition (\%) = 100 \left(\frac{A_{405} NegControl - A_{405} Sample}{A_{405} NegControl} \right)$$

Untargeted metabolomic analyses

The chromatographic system was an UPLC Class I of Waters coupled to a Synapt G2Si HDMi mass spectrometer. The chromatography was carried out on an Acquity BEH column (1.7 μ m, 2.1 x 50 mm) with a column and sample temperatures of 40°C and 15°C, respectively. The mobile phase consisted of (A) water and (B) acetonitrile, both with 0.1% of formic acid (Sigma-Aldrich, St Louis, MO, USA). The gradient conditions of the mobile phases were 0–20 min linear gradient 1–99% B, 20–24 min 99% B isocratic, 24–25 min linear gradient 90 – 1% B and total run time of 30 min. The flow rate was 0.3 mL/min and 5 μ L of extract was injected. The mass spectrometric analysis was performed with an electrospray ionization (ESI) source in positive mode with a capillary, sampling cone and source offset voltages of 3000, 40 and 80 V, respectively. The source temperature was 120°C and the desolvation temperature was 20°C. The desolvation gas flow was 600 L/h and the nebulizer pressure was 6.5 Bar. Leucine-enkephalin was used as the lock mass (556.2771, [M + H]⁺). The conditions used for MS analysis were: mass range 50-1200 Da, Function 1 CE, 6 V, function 2 CER 10–30 V, scan time 0.5 sec. Data were acquired and processed with MassLynx (version 4.1, Waters, Milford, MA, USA) and MarkerLynx (version 4.1, Waters, Milford, MA, USA) software.

Comparative analysis

The retention times (Rt) and the mass-charge ratios (m/z) in positive ionization mode (ESI⁺) were generated at a noise threshold of 500 counts and peak smoothing was applied. The raw data were exported to Excel (Microsoft Software) tables for statistical analysis. MetaboAnalyst platform (V. 5.0; Xia & Wishart, (2016); <https://www.metaboanalyst.ca/>), through its different modules, was used for the functional analysis of untargeted metabolomic data. Using the statistical analysis module, multivariate methods were used to compare the samples. The intensity of the Rt- m/z signals was transformed (Log₁₀) and normalized by Pareto scale. The heatmap with hierarchical clustering (HCA) and the principal component analysis (PCA) were carried out with the ESI⁺ dataset matrix. Heatmap and PCA were performed to determine the similarity between samples according to their chemical composition. Paired comparative analyses were performed to identify over and down-accumulated metabolites [Fold Change (FC) values ≥ 1.5 or ≤ 0.67 , respectively]. Results were presented by plotting p -values against the log(10) for the fold change values on a volcano plot for each signal detected as statistically differential for each treatment.

The spectrometric features (Rt- m/z) signals were tentatively identified using the functional analysis module considering the *Arabidopsis thaliana* metabolome from KEGG as reference. To carry out the impact

of metabolic pathways in all treatments, the algorithms of Mummichog and GSEA of the MetaboAnalyst platform were used. The Venn diagram was generated with the Venny Platform (V. 2.1; <https://bioinfogp.cnb.csic.es/tools/venny/index.html>).

Molecular docking

The chemical structures of over-accumulated compounds identified by mass spectrometry from treatments Tyr_100 and Tyr_200 were obtained from the PubChem compound database (<https://pubchem.ncbi.nlm.nih.gov>). Only compounds detected with a FC greater than 500 were used. Ligands were prepared by adding polar hydrogens and saving them in PDB format using Discovery Studio 2021 (Dassault Systemes, France). PDB files were processed for charges and torsions and then converted into PDBQT files using Autodock Tools (Morris, 2009). The three-dimensional crystal structure of α -amylase (PDB ID: 1OSE) in complex with co-crystallized ligand, acarbose, was retrieved from the Protein Data Bank (<http://www.rcsb.org/pdb>). The protein was prepared using Discovery Studio 2021 to remove nonessential water molecules, cofactors, and ions. Additionally, the co-crystallized ligand was extracted from the active site of the protein to reveal the grid coordinate around the binding pocket which corresponded to the catalytic cavity ($x = 33.7, y = 36.4, z = 3.9$). Finally, the protein PDB file was converted to PDBQT format using Autodock Tools (Morris, 2009). Following protein target and ligand preparation, molecular docking analysis were performed using Autodock Vina (Trott & Olson, 2010). The resulting interactions were analyzed and compared, and the pose with the lowest binding free energy (BFE) was chosen as the most suitable. Images were generated using Discovery Studio 2021.

RESULTS AND DISCUSSION

Inhibition of α -amylase

R. echinocarpa methanolic extracts inhibited α -amylase enzymatic activity, corresponding to the first step in for the hydrolysis of starch and other carbohydrate polymers into shorter oligosaccharides. The α -amylase inhibitory effect of the extracts tested at 1 mg/mL was significantly similar to, or greater than the observed for acarbose at 25 mM (Table 1). Extracts from Tyr_50 and 100 had better ($p < 0.05$) inhibitory activity than the control (Ctrl); while the obtained for Tyr_200 ($34.20 \pm 0.38\%$) was similar ($p > 0.05$) to acarbose 50 mM ($32.36 \pm 1.85\%$). Extracts from other plants and algae have also shown similar activities (Picos-Salas et al., 2021; Landa-Cansigno et al., 2020). When tested at 400 μ g/mL, extracts from *Lippia graveolens* inhibited α -amylase by 43.41% while those from *Lippia palmieri* did it only by 12.19% (Gutiérrez-Grijalva et al., 2019). Methanolic extracts of *Vernonia antihelmitica* callus and leaf showed an IC_{50} of 0.499 mg/L and 0.372 mg/L, respectively (Rajan et al., 2022). Moderate inhibition (30–50%) of α -amylase is desired since excessive bacterial fermentation of non-digested carbohydrates in colon could cause diarrhea and flatulence (Kashtoh & Baek, 2023).

Inhibition of α -glucosidase

Contrasting to the α -amylase activities described above, no enzymatic inhibition was observed for α -glucosidase (data not shown). A previous study carried out by Cuevas-Juárez et al. (2014), reported that partially purified melanins from the pulp fruit of *R. echinocarpa* presented higher α -glucosidase inhibitory (IC_{50} 1.00–1.17 mg/mL) activities when compared with acarbose (8.38 mg/mL). On the other hand, different plant extracts showed better inhibitory activity on α -amylase than the observed for α -glucosidase. Hua et al. (2018) reported flavone glycosides isolated from Lu'an GuaPian tea (*Camelia sinensis* L.O. Kuntze) with better inhibition effects on α -amylase (IC_{50} 0.50–12.05 μ M) than for α -glucosidase (IC_{50} 28.11–106.65 μ M). Similarly, different fractions from *Persicaria hydropiper* presented higher inhibition activities on α -amylase than α -glucosidase (Mahnashi et al., 2022). The IC_{50} of a methanolic extract of *V. antihelmitica* callus was also higher for α -glucosidase inhibition than the observed for α -amylase (Rajan et al., 2022). Methanolic extracts of *Carthamus tinctorius* callus showed a IC_{50} for α -glucosidase of 0.63 g/L that was mainly attributed to the presence of different chlorogenic acids (Liu et al., 2023). The fact that only α -amylase activity was inhibited by the methanolic extracts of *R. echinocarpa* can be attributed to the complex mixture, and to synergic or antagonist effects of the compounds (Landa-Cansigno et al., 2020).

Table 1
Inhibition of α -amylase by crude extracts (1 mg/mL) of *R. echinocarpa* cell suspensions treated with 50, 100 or 200 mg/L of L-tyrosine compared to acarbose 25–150 μ M.

Treatment	Inhibition of α -amylase (%)
Ctrl	13.90 \pm 1.43 e
Tyr_50	20.84 \pm 0.83 d
Tyr_100	24.79 \pm 1.27 d
Tyr_200	34.20 \pm 0.38 c
25 μ M Acarbose	9.46 \pm 3.06 e
50 μ M Acarbose	32.36 \pm 1.85 c
100 μ M Acarbose	61.87 \pm 1.14 b
150 μ M Acarbose	69.20 \pm 1.25 a

Ctrl, control; Tyr_50, L-tyrosine at 50 mg/L; Tyr_100, L-tyrosine at 100 mg/mL; Tyr_200, L-tyrosine at 200 mg/L.

Hierarchical Clustering Analysis

Mass spectrometric analysis detected 494 R_t - m/z signals in positive mode. The addition of Tyr at different concentrations induced significant changes in the chemical profile of the *R. echinocarpa* cell suspensions (Fig. 1a). In general, control sample (Ctrl) showed decreased (blue) intensities of the R_t - m/z signals compared to the Tyr treatments. Tyr_100 and Tyr_200 treatments showed similar signal intensities. This

was further supported by the 3D-PCA diagrams, whose components explained 95.2% of the total variance (Fig. 1b). To represent the number of statistically significant Rt-*m/z* signals shared between Tyr treatments, a Venn diagram was created (Fig. 1c). The core metabolism consisted of 221 Rt-*m/z* signals. Tyr₁₀₀ treatment presented the highest number of unique Rt-*m/z* signals (59), while Ctrl presented the lowest number of Rt-*m/z* signals (44). In a similar way, Ctrl and Tyr₅₀ treatments showed similar number of unique Rt-*m/z* signals with 44 and 45, respectively. These changes in the intensities detected represent the changing accumulation of the compounds due to the activation, or inactivation, of different metabolic pathways.

Enrichment of Metabolic Pathways

In Table S1, the total number of metabolites in the pathway and the number of metabolites identified in the data (hits) were summarized along with the raw *p*-value calculated from the enrichment analysis and the impact value. The functional analysis considering all signals detected by the metabolomic approach serves to identify the main metabolic pathways (pathway impact values ≥ 0.15 and *p*-values ≤ 0.1) present in the cell suspensions of *R. echinocarpa* from all treatments (Fig. 2).

Galactose and starch/sucrose metabolism were among the main metabolic pathways identified by the functional analysis (Fig. 2); both are involved in the over-accumulation of compounds related with carbohydrate utilization. Other metabolic pathways affected by the Tyr treatments included steroid biosynthesis, ubiquinone and other terpenoid-quinone biosynthesis, sphingolipid metabolism and Tyr metabolism. It was expected an increase in the metabolism of Tyr and other metabolic pathways involved in its utilization, like the biosynthesis of ubiquinone and other terpenoid-quinones, since Tyr serves as a precursor for the biosynthesis of specialized metabolites involved in those metabolic pathways (Xu et al., 2020).

The brassinosteroid and steroid biosynthesis, and the sphingolipid metabolism pathways were also identified in the *R. echinocarpa* cell suspensions treated with Tyr. Brassinosteroids are considered the sixth class of plant regulators, being present in all plant organs, and have a fundamental role in the development and growth of plants, inducing a wide range of morphological and physiological responses, including tolerance against abiotic and biotic stress (Bajguz et al., 2020; Wei & Li, 2020). On the other hand, in plants, cell membranes are primarily composed of glycerolipids, sterols and sphingolipids (Valitova et al., 2016), thus the high impact on the steroid biosynthesis and the sphingolipid metabolism in the cell suspensions of *R. echinocarpa* was also expected to occur. Plant sterols are used for the biosynthesis of brassinosteroids (Sonawane et al., 2016). On the other hand, sphingolipids are also crucial for maintaining the morphology of membrane systems and modulating membrane functions like signaling, cell polarity, and cellular responses to abiotic and biotic conditions (Haslam & Feussner, 2022).

The metabolites over-accumulated in the Tyr₁₀₀ and 200 methanolic extracts, in comparison to Ctrl, were tentatively identified and enlisted in Table 2. In Tyr₁₀₀, the compound with the highest FC value (3343) was homovanillic acid 4-glucuronide, while in Tyr₂₀₀ the highest FC value (622.36) corresponds to 5'-phosphoribosyl-N-formylglycinamide, a compound also identified in Tyr₁₀₀. Wang et al. (2019) reported

an increase of homovanillic along with salicylic, caffeic, and ferulic acids after short-term heat shock treatment in *Festuca trachyphylla*. On the other hand, application of LED light stimulated the production of several phenolics, including homovanillic acid, in seedlings of *Fagopyrum esculentum* Moench (Hornyák et al., 2022).

In plants, Tyr can be consumed to synthesize L-DOPA, a precursor of homovanillic acid, and it has been reported as an important regulator of the synthesis of specialized metabolites like those derived from the phenylpropanoid pathway (Breitel et al., 2021). Although the presence of L-DOPA was not observed as an accumulated compound in the methanolic extracts, this can be attributed to its utilization for the synthesis of homovanillic acid. Moreover, other compounds can be synthesized from L-DOPA, such as melanins (Soares et al., 2014). In this metabolic branch, Tyr is oxidized to L-DOPA by the enzyme tyrosinase oxidase (TYROX), which is also involved in the synthesis of melanins (Oviedo-Silva et al., 2018). Melanins can also be produced by enzymatic browning reactions catalyzed by polyphenol oxidases (PPOs) from phenolic substrates (Glagoleva et al., 2020).

The tentative identification of flavonoid-o-glycosides, oligosaccharides, methyl 3,4-dicaffeoylquinic acid, and diferuloylquinic acid, was also observed in Tyr_100. Further analyses with standards are required to corroborate the presence of these compounds in the methanolic extracts of *R. echinocarpa* cell suspensions. Flavonoids have been reported to inhibit α -amylase (Martínez-González et al., 2019). This inhibition is attributed to the ability of flavonoids to interact with proteins, either with covalent or non-covalent bonds (Takahama & Hirota, 2018).

Among the compounds that were upregulated by Tyr at 200 or 100 mg/L, 5'-phosphoribosyl-N-formylglycineamide had a fold change (FC) of 624.4 and 608, respectively. This compound is involved in purine pathway. Inositol derivatives were over accumulated only increased in Tyr_200 by a FC of 124.3. Martínez-Ceja et al. (2022) reported the presence of inositol in the methanolic extracts of *R. aculeata* L.

Hexadecanoic acid (palmitate) was previously reported in hexane and dichloromethane extracts of *Randia aculeata* L. cell suspensions (Martínez-Ceja et al., 2022). Hexadecanoic acid had a FC of 6.6 in Tyr_200. In Tyr_100, methylhexadecanoic acid had a FC of 16.2. Previous studies had reported the inhibitory effects of hexadecanoic acid on the activities of α -amylase (Hoang-Anh et al., 2020) and α -glucosidase (Su et al., 2013). Isoflavones and palmitic acid derivatives have been reported to inhibit α -amylase activity (Martínez-González et al., 2019; Hoang-Anh et al., 2020). Thus, the increased inhibition of this enzyme by the Tyr_200 can be related with the over-accumulation of these compounds in the *R. echinocarpa* cell suspensions.

Table 2

Tentative identification of the over-accumulated compounds in Tyr_100 and Tyr_200 treatments in comparison to control (Ctrl).

Treatment	Rt	m/z	FC	p value	Tentative compound	Adduct	Error (ppm)
Tyr_100	0.47	104.1069	230.0	0.0350	Choline	[M + H] ⁺	6
	0.5	381.0783	3343.0	0.0545	Homovanillic acid 4-glucuronide	[M + Na] ⁺	2
	0.51	191.039	591.2	0.0427	L-Glutamine	[M + 2Na - H] ⁺	6
	0.51	279.0383	608.0	0.0429	5'-Phosphoribosyl-N-formylglycinamide	[M + H - 2H ₂ O] ⁺	2
	0.51	527.1569	2249.8	0.0519	Flavonoid-o-glycosides, oligosaccharides, Methyl 3,4-dicaffeoylquinic acid, Diferuloylquinic acid,	[M + H - H ₂ O] ⁺ , [M + Na] ⁺	3
	0.53	185.0419	527.9	0.0418	1-Rhamnono-1,4-lactone	[M + Na] ⁺	1
	0.53	321.0495	1146.1	0.0475	Imidazoleacetic acid ribotide, Alanine-betaxanthin	[M + H - H ₂ O] ⁺ , [M + K] ⁺	2, 4
	0.54	427.075	1681.9	0.0500	Ferulic acid	[2M + K] ⁺	9
	10.15	288.2893	16.2	2.922e-06	Methylhexadecanoic acid	[M + NH ₄] ⁺	1
	11.51	453.1667	5.8	1.712e-05	Flavanones	[M + 2Na - H] ⁺	4
	11.81	302.305	5.5	4.601e-09	Sphinganine	[M + H] ⁺	1
	14.44	349.1352	5.9	0.0004	N2-(2-Carboxymethyl-2-hydroxysuccinoyl)arginine	[M + H] ⁺	1

Treatment	Rt	<i>m/z</i>	FC	<i>p</i> value	Tentative compound	Adduct	Error (ppm)
Tyr_200	0.5	369.0719	188.5	3.30e-02	L-Dopachrome, Isoflavonoids	[2M + H- H ₂ O] ⁺ , [M + K] ⁺	0, 4
	0.5	219.0179	362.2	3.88e-02	Fatty acids	[M + 2K] ⁺	2
	0.51	279.0383	622.4	4.31e-02	5'-Phosphoribosyl-N-formylglycinamide	[M + H- 2H ₂ O] ⁺	2
	0.53	335.0938	154.0	3.21e-02	O-glycosyl compounds, flavonoids, Imidazolelactate	[M + H- H ₂ O] ⁺	5
	0.53	185.0419	174.0	3.22e-02	1-Rhamnono-1,4-lactone	[M + Na] ⁺	1
	0.54	203.0525	124.3	2.89e-02	Monosaccharides, Inositol derivatives	[M + Na] ⁺	3
	10.09	274.2738	6.6	1.45e-04	Palmitic acid, isopalmitic acid	[M + NH ₄] ⁺	1
	11.51	453.1667	5.5	3.50e-06	Flavanones	[M + 2Na- H] ⁺	4
	14.44	349.1352	5.6	5.97e-06	N ₂ -(2-Carboxymethyl-2-hydroxysuccinoyl)arginine	[M + H] ⁺	N/A

Tyr_100: L-tyrosine at 100 mg/L; Tyr_200: L-tyrosine at 200 mg/L; Rt: retention time in minutes; *m/z*: mass/charge in Daltons; FC: fold change.

Molecular docking

The molecular docking analysis revealed that compounds identified in *R. echinocarpa* cell cultures could interact with several amino acid residues within the α -amylase catalytic site. These compounds exhibited predicted energy binding values ranging from - 5.6 to -3.4 kcal/mol, which are considered stable interactions (Yañez-Apam et al., 2023). These results were in accordance with estimated free binding energies predicted among α -amylase and small molecules such as flavonoid or pirazole derivatives (Rydberg et al., 2002; Mai et al., 2023). The enzyme α -amylase exists in two isoforms, present in both saliva and pancreatic secretions (Freitas et al., 2023). Both isoforms are composed of 496 amino acids and could be divided into three different domains (A, B, and C), with the catalytic triad (Asp197, Glu233, and Asp300) responsible for the cleaving function of the enzymes located in the A domain. Since the center of the

binding site is exposed to the center of a large cavity that is found on the side of the A domain, it is more likely for smaller structures to access the binding site (Rydberg et al., 2002). The stereochemistry appears to play a role in the biological activity of the compounds inhibiting α -amylase (Akshatha et al., 2021). The compounds identified in *R. echinocarpa*, specially homovanillic acid 4-glucuronide, cultures were able to interact with several binding site residues of the enzyme; therefore, they may be able to pose in the large cavity blocking access to the substrate (Fig. 3A). The interactions between α -amylase and this compound were able to generate a hydrophobicity surface (Fig. 3B) that stabilizes the ligand within the catalytic pocket of the enzyme, and the types of interactions found were mainly H-bond, hydrophobic, and π bonds as observed in Fig. 3C. Acarbose was used as a control, showing a predicted energy binding value of -8.4 kcal/mol and demonstrated the most diverse interactions within the catalytic cavity of α -amylase (Table 3). The compounds identified in *R. echinocarpa* cell culture treated with Tyr_100 with a FC greater than 500 (homovanillic acid 4-glucuronide, 5'-phosphoribosyl-N-formylglycinamide, diferuloylquinic acid, ferulic acid, and imidazoleacetic acid ribotide) had an estimated free binding energy of -2.4 to -5.6 kcal/mol. On the other hand, only one compound in the treatment with Tyr_200 were identified to have a greater FC of 500, with estimated free binding energies of -5.3 kcal/mol. Notably, 5'-phosphoribosyl-N-formylglycinamide were able to interact with Asp300, a key amino acid in the deformation of the α -amylase substrate and enhancement of sugar electrophilicity during nucleophilic attacks during the first steps of the enzymatic reaction degrading carbohydrates (Rydberg et al., 2002). The fact that Tyr_100 showed lower inhibitory activity in α -amylase than Tyr_200 can be attributed to the presence of other compounds with antagonist effects, as discussed previously.

Table 3. Estimated free energy binding and interacting amino acids among the compounds present in cell culture of *R. echinocarpa* treated with 100 or 200 mg/L of tyrosine and the catalytic site of α -amylase.

Compound	EBE (kcal/mol)	Interacting amino acids in the catalytic site
Homovanillic acid 4-glucuronide	-5.6	Tyr62, Gln63, Asp96
5'-Phosphoribosyl-N-formylglycinamide	-5.3	Trp59, Tyr62, Gln63, Leu162, Asp300
Diferuloylquinic acid	-3.5	Asp197, Ala198, Val234
Ferulic acid	-3.4	Tyr62, Gln63, Asp300, Gly306
1-Rhamnono-1,4-lactone	1.3	-
Acarbose	-8.4	Hist101, Gln63, Leu165, Tyr62, Ala198, Asp300, Glu233, His299, Leu162, His305, Trp59, Val163, Trp357, Asp356, His201, Gly306, Ile235, Trp58, Lys200, Tyr151

EBE: estimated free binding energy, Trp: tryptophane, Tyr: tyrosine, Gln: glutamine, Val: valine, Asp: asparagine, Ala: alanine, Leu: leucine, His: histidine.

CONCLUSIONS

The addition of 50, 100 or 200 mg/L of tyrosine induced changes in the chemical profile of the *R. echinocarpa* cell cultures. Moreover, the cell extracts inhibited the activity of α -amylase, though no inhibition was observed in the activity of α -glucosidase. The results herein presented made headway to understand the changes in the *R. echinocarpa* chemical profile and to develop efficient strategies to increase the production of specialized metabolites with specific biological activities. Compounds like homovanillic acid 4-glucuronide and diferuloylquinic acid were over-accumulated and as 5'-phosphoribosyl-N-formylglycinamide could be overproduced in *R. echinocarpa* cell cultures to produce α -amylase inhibitory extracts.

Declarations

ACKNOWLEDGEMENTS

The authors thank CIIDIR-IPN Sinaloa Unit for providing the *Randia echinocarpa* seeds.

FUNDING INFORMATION

This work was financially supported by the "Consejo Nacional de Humanidades, Ciencia y Tecnología (CONAHCYT)" for the scholarship 2019-000037-02NACF-07262 and by the "Instituto Tecnológico de Estudios Superiores de Monterrey" for the Challenge Based Research Fund "Smart Lipids -conjugates with antioxidant proteins and starch to reduce glycaemic index and deliver lipophilic anti-obesogenic compounds to develop a healthy food for children and their families".

AUTHOR CONTRIBUTION

Miguel Aguilar-Camacho: Conceptualization, experimental work, data analysis, writing - original draft. Carlos Eduardo Gómez-Sánchez, Abraham Cruz-Mendivil, Diego Luna, José A Guerrero-Analco, Juan L. Monribo-Villanueva: support during experimental work and formal analysis. Janet A. Gutiérrez-Urbe: conceptualization, funding acquisition, experimental design, project administration, supervision, manuscript review and edition.

CONFLICT OF INTEREST

The authors have no competing interests to declare that are relevant to the content of this article

DATA AVAILABILITY

Data will be made available on reasonable request.

References

1. Aguilar-Camacho M, Gómez-Sánchez CE, Cruz-Mendivil A, Guerrero-Analco JA, Monribot-Villanueva JL, Gutiérrez-Urbe J (2023) Modeling the growth kinetics of cell suspensions of *Randia echinocarpa* and characterization of their bioactive phenolic compounds. *Plant Cell Tiss Organ Cult* 155:785–796. <https://doi.org/10.21203/rs.3.rs-2909503/v1>
2. Akshatha JV, SantoshKumar HS, Prakash HS, Nalini MS (2021) In silico docking studies of α -amylase inhibitors from the anti-diabetic plant *Leucas ciliata* Benth. and an endophyte, *Streptomyces longisporoflavus*. *3 Biotech* 11:1–16. <https://doi.org/10.1007/s13205-020-02547-0>
3. Bajguz A, Chmur M, Gruszka D (2020) Comprehensive overview of the brassinosteroid biosynthesis pathways: substrates, products, inhibitors, and connections. *Front Plant Sci* 11:1034. <https://doi.org/10.3389/fpls.2020.01034>
4. Balažová A, Urdová J, Forman V, Mučaji P (2020) Enhancement of macarpine production in *Eschscholzia californica* suspension cultures under salicylic acid elicitation and precursor supplementation. *Molecules* 25(6):1261. <https://doi.org/10.3390/molecules25061261>
5. Biswas T, Mathur A, Gupta V, Luqman S, Mathur AK (2020) Elicitation and phenylalanine precursor feeding based modulation of in vitro anthocyanin production, enzyme activity and gene expression in an Indian ginseng congener-*Panax sikkimensis* Ban. *Ind Crops Prod* 145:111986. <https://doi.org/10.1016/j.indcrop.2019.111986>
6. Breitel D, Brett P, Alseekh S, Fernie AR, Butelli E, Martin C (2021) Metabolic engineering of tomato fruit enriched in L-DOPA. *Metabolic Eng* 65:185–196. <https://doi.org/10.1016/j.ymben.2020.11.011>
7. Cano-Campos MC, Díaz-Camacho SP, Uribe-Beltran M, López-Angulo G, Montes-Avila J, Paredes-López O, Delgado-Vargas F (2011) Bio-guided fractionation of the antimutagenic activity of methanolic extract from the fruit of *Randia echinocarpa* (Sessé et Mociño) against 1-nitropyrene. *Food Res Int* 44(9):3087–3093. <https://doi.org/10.1016/j.foodres.2011.08.006>
8. Chandrasekaran S, Luna-Vital D, de Mejia EG (2020) Identification and comparison of peptides from chickpea protein hydrolysates using either bromelain or gastrointestinal enzymes and their relationship with markers of type 2 diabetes and bitterness. *Nutrients* 12(12):3843. <https://doi.org/10.3390/nu12123843>
9. Cortés F (2000) Medicine, myths and magic the folk healers of a Mexican market. *Econ Bot* 54:427–438. <https://doi.org/10.1007/BF02866542>
10. Cuevas-Juárez E, Yurjar-Arredondo KY, Pío-León JF, Montes-Avila J, López-Angulo G, Díaz-Camacho SP, Delgado-Vargas F (2014) Antioxidant and α -glucosidase inhibitory properties of soluble melanins from the fruits of *Vitex mollis* Kunth, *Randia echinocarpa* Sessé et Mociño and *Crescentia alata* Kunth. *J Funct Foods* 9:78–88. <https://doi.org/10.1016/j.jfff.2014.04.016>
11. Feduraev P, Skrypnik L, Riabova A, Pungin A, Tokupova E, Maslennikov P, Chupakhina G (2020) Phenylalanine and tyrosine as exogenous precursors of wheat (*Triticum aestivum* L.) secondary metabolism through PAL-associated pathways. *Plants* 9(4):476. <https://doi.org/10.3390/plants9040476>
12. Freitas M, Proença C, Ribeiro D, Quinaz-Garcia MB, Araújo AN, Fernandes E (2023) Assessment of α -amylase activity in a microanalysis system: Experimental optimization and evaluation of type of

- inhibition. *J Chem Educ* 100(3):1237–1245. <https://doi.org/10.1021/acs.jchemed.2c00392>
13. Gabotti D, Locatelli F, Cusano E, Baldoni E, Genga A, Pucci L, Consonni R, Mattana M (2019) Cell suspensions of *Cannabis sativa* (var. futura): Effect of elicitation on metabolite content and antioxidant activity. *Molecules* 24(22): 4056. <https://doi.org/10.3390/molecules24224056>
 14. Glagoleva AY, Shoeva OY, Khlestkina EK (2020) Melanin pigment in plants: Current knowledge and future perspectives. *Front Plant Sci* 11:770. <https://doi.org/10.3389/fpls.2020.00770>
 15. Gómez-Tah R, Islas-Flores I, Félix JW, Granados-Alegría MI, Tzec-Simá M, Guerrero-Analco JA, Monribo-Villanueva JL, Canto-Canché B (2023) Untargeted metabolomics analysis of liquid endosperm of *Cocos nucifera* L. at three stages of maturation evidenced differences in metabolic regulation. *Horticulturae* 9(8):866. <https://doi.org/10.3390/horticulturae9080866>
 16. Gutiérrez-Grijalva EP, Antunes-Ricardo M, Acosta-Estrada BA, Gutiérrez-Urbe JA, Heredia JB (2019) Cellular antioxidant activity and in vitro inhibition of α -glucosidase, α -amylase and pancreatic lipase of oregano polyphenols under simulated gastrointestinal digestion. *Food Res Inter* 116:676–686. <https://doi.org/10.1016/j.foodres.2018.08.096>
 17. Haslam TM, Feussner I (2022) Diversity in sphingolipid metabolism across land plants. *J Exp Bot* 73(9):2785–2798. <https://doi.org/10.1093/jxb/erab558>
 18. Hegazi GA, Ibrahim WM, Hendawy MH, Salem HM, Ghareb HE (2020) Improving α -tocopherol accumulation in *Argania spinosa* suspension cultures by precursor and nanoparticles feeding. *Plant Arch* 20:2431–2437
 19. Hoang Anh L, Xuan TD, Dieu Thuy NT, Quan NV, Trang LT (2020) Antioxidant and α -amylase inhibitory activities and phytochemicals of *Clausena indica* fruits. *Medicines* 7(3):10. <https://doi.org/10.3390/medicines7030010>
 20. Hornyák M, Dziurka M, Kula-Maximenko M, Pastuszak J, Szczerba A, Szklarczyk M, Płażek A (2022) Photosynthetic efficiency, growth and secondary metabolism of common buckwheat (*Fagopyrum esculentum* Moench) in different controlled-environment production systems. *Sci Rep* 12(1):257. <https://doi.org/10.1038/s41598-021-04134-6>
 21. Hua F, Zhou P, Wu HY, Chu GX, Xie ZW, Bao GH (2018) Inhibition of flavonoid glycosides from Lu'an GuaPian tea on α -glucosidase and α -amylase: Molecular docking and interaction mechanism. *Food Funct* 9:4173–4183. <https://doi.org/10.1039/C8FO00562A>
 22. Isah T, Umar S, Mujib A, Sharma MP, Rajasekharan PE, Zafar N, Fruk A (2017) Secondary metabolism of pharmaceuticals in the plant *in vitro* cultures: strategies, approaches, and limitations to achieving higher yield. *Plant Cell Tiss Organ Cult* 132:239–265. <https://doi.org/10.1007/s11240-017-1332-2>
 23. Jacobowitz JR, Weng JK (2020) Exploring uncharted territories of plant specialized metabolism in the postgenomic era. *Annual Rev Plant Biol* 71:631–658. <https://doi.org/10.1146/annurev-arplant-081519-035634>
 24. Juárez-Trujillo N, Monribo-Villanueva JL, Alvarado-Olivarez M, Luna-Solano G, Guerrero-Analco JA, Jiménez-Fernández M (2018) Phenolic profile and antioxidative properties of pulp and seeds of *Randia monantha* Benth. *Ind Crops Prod* 124:53–58. <https://doi.org/10.1016/j.indcrop.2018.07.052>

25. Kashtoh H, Baek KH (2023) New insights into the latest advancement in α -amylase inhibitors of plant origin with anti-diabetic effects. *Plants* 12(16):2944. <https://doi.org/10.3390/plants12162944>
26. Landa-Cansigno C, Hernández-Domínguez EE, Monribot-Villanueva JL, Licea-Navarro AF, Mateo-Cid LE, Segura-Cabrera A, Guerrero-Analco JA (2020) Screening of Mexican tropical seaweeds as sources of α -amylase and α -glucosidase inhibitors. *Algal Res* 49:101954. <https://doi.org/10.1016/j.algal.2020.101954>
27. Liu Z, Du L, Liu N, Mohsin A, Zhu X, Sun H, Zhou B, Yin Z, Zhuang Y, Guo M, Wang Z (2023) Insights into chlorogenic acids' efficient biosynthesis through *Carthamus tinctorius* cell suspension cultures and their potential mechanism as α -glucosidase inhibitors. *Ind Crops Prod* 194:116337. <https://doi.org/10.1016/j.indcrop.2023.116337>
28. López-Berenguer C, Donaire L, González-Ibeas D, Gómez-Aix C, Truniger V, Pechar GS, Aranda MA (2021) Virus-infected melon plants emit volatiles that induce gene deregulation in neighboring healthy plants. *Phytopathology* 111(5):862–869. <https://doi.org/10.1094/PHTO-07-20-0301-R>
29. Mahnashi MH, Alqahtani YS, Alyami BA, Alqarni AO, Alqahl SA, Ullah F, Sadiq A, Zeb A, Ghufuran M, Kuraev A, Nawaz A, Ayaz M (2022) HPLC-DAD phenolics analysis, α -glucosidase, α -amylase inhibitory, molecular docking and nutritional profiles of *Persicaria hydropiper* L. *BMC Complement Med Ther* 22(1):26. <https://doi.org/10.1186/s12906-022-03510-7>
30. Mai TT, Phan MH, Thai TT, Lam TP, Lai NVT, Nguyen TT, Nguyen TVP, Thi Vo CV, Thai KM, Tran TD (2023) Discovery of novel flavonoid derivatives as potential dual inhibitors against α -glucosidase and α -amylase: virtual screening, synthesis, and biological evaluation. *Mol Divers* 1–22. <https://doi.org/10.1007/s11030-023-10680-0>
31. Maidadi B, Ntchapda F, Miaffo D, Kamgue Guessom O (2022) Efficacy of *Rytigynia senegalensis* Blume on free radical scavenging, inhibition of α -amylase and α -glucosidase activity, and blood glucose level. *Evidence-Based Complementary and Alternative Medicine*, 2022. <https://doi.org/10.1155/2022/9519743>
32. Martínez-Ceja A, Romero-Estrada A, Columba-Palomares MC, Hurtado-Díaz I, Alvarez L, Teta-Talixtacta R, Sánchez-Ramos M, Cruz-Sosa F, Bernabé-Antonio A (2022) Anti-inflammatory, antibacterial and antioxidant activity of leaf and cell cultures extracts of *Randia aculeata* L. and its chemical components by GC-MS. *South Afr J of Botany* 144:206–218. <https://doi.org/10.1016/j.sajb.2021.08.036>
33. Martínez-González AI, Díaz-Sánchez ÁG, De La Rosa LA, Bustos-Jaimes I, Alvarez-Parrilla E (2019) Inhibition of α -amylase by flavonoids: Structure activity relationship (SAR). *Spectrochim Acta A Mol Biomol Spectrosc* 206:437–447. <https://doi.org/10.1016/j.saa.2018.08.057>
34. Mojica L, Luna-Vital DA, González de Mejía E (2016) Characterization of peptides from common bean protein isolates and their potential to inhibit markers of type-2 diabetes, hypertension and oxidative stress. *J Sci Food Agric* 97(8):2401–2410. <https://doi.org/10.1002/jsfa.8053>
35. Montes-Avila J, Ojeda-Ayala M, López-Angulo G, Pío-León JF, Díaz-Camacho SP, Ochoa-Terán A, Delgado-Vargas F (2018) Physicochemical properties and biological activities of melanins from the

- black-edible fruits *Vitex mollis* and *Randia echinocarpa*. J Food Meas Charact 12:1972–1980.
<https://doi.org/10.1007/s11694-018-9812-6>
36. Morris GM, Huey R, Lindstrom W, Sanner MF, Belew RK, Goodsell DS, Olson AJ (2009) AutoDock4 and AutoDockTools4: Automated docking with selective receptor flexibility. J Comp Chem 30(16):2785–2791. <https://doi.org/10.1002/jcc.21256>
 37. Murashige T, Skoog F (1962) A revised medium for rapid growth and bio assays with tobacco tissue cultures. Physiol Plant 15(3):473–497. <https://doi.org/10.1111/j.1399-3054.1962.tb08052.x>
 38. Oviedo-Silva CA, Elso-Freudenberg M, Aranda-Bustos M (2018) L-DOPA trends in different tissues at early stages of *Vicia faba* growth: effect of tyrosine treatment. Appl Scis 8(12):2431. <https://doi.org/10.3390/app8122431>
 39. Picos-Salas MA, Gutiérrez-Grijalva EP, Valdez-Torres B, Angulo-Escalante MA, López-Martínez LX, Delgado-Vargas F, Basilio-Heredia J (2021) Supercritical CO₂ extraction of oregano (*Lippia graveolens*) phenolic compounds with antioxidant, α-amylase and α-glucosidase inhibitory capacity. Food Measure 15:3480–3490. <https://doi.org/10.1007/s11694-021-00928-4>
 40. Pillai SK, Siril EA (2022) Exogenous elicitors enhanced berberine production in the cell suspension cultures of *Tinospora cordifolia* (Willd.) Miers ex Hook F. & Thoms. Proc Natl Acad Sci, India, Sect B Biol Sci 92: 209–218. <https://doi.org/10.1007/s40011-021-01310-6>
 41. Rajan M, Chandran V, Shahena S, Anie Y, Mathew L (2022) *In vitro* and *in silico* inhibition of α-amylase, α-glucosidase, and aldose reductase by the leaf and callus extracts of *Vernonia anthelmintica* (L.) Willd. Advances in Traditional Medicine: 1–15. <https://doi.org/10.1007/s13596-020-00533-8>
 42. Rydberg EH, Li C, Maurus R, Overall CM, Brayer GD, Withers SG (2002) Mechanistic analyses of catalysis in human pancreatic α-amylase: Detailed kinetic and structural studies of mutants of three conserved carboxylic acids. Biochem 41(13):4492–4502. <https://doi.org/10.1021/bi011821z>
 43. Santos-Cervantes ME, Ibarra-Zazueta ME, Loarca-Piña G, Paredes-López O, Delgado-Vargas F (2007) Antioxidant and antimutagenic activities of *Randia echinocarpa* fruit. Plant Foods Hum Nutr 62:71–77. <https://doi.org/10.1007/s11130-007-0044-x>
 44. Schenck CA, Maeda HA (2018) Tyrosine biosynthesis, metabolism, and catabolism in plants. Phytochem 149:82–102. <https://doi.org/10.1016/j.phytochem.2018.02.003>
 45. Simpson JP, Olson J, Dilkes B, Chapple C (2021) Identification of the tyrosine-and phenylalanine-derived soluble metabolomes of sorghum. Front Plant Sci 12:714164. <https://doi.org/10.3389/fpls.2021.714164>
 46. Soares AR, Marchiosi R, Siqueira-Soares RDC, Barbosa de Lima R, Dantas dos Santos W, Ferrarese-Filho O (2014) The role of L-DOPA in plants. Plant Signal Behav 9(4):e28275. <https://doi.org/10.4161/psb.28275>
 47. Sonawane PD, Pollier J, Panda S et al (2016) Plant cholesterol biosynthetic pathway overlaps with phytosterol metabolism. Nat Plants 3(1):1–13
 48. Su CH, Hsu CH, Ng LT (2013) Inhibitory potential of fatty acids on key enzymes related to type 2 diabetes. BioFactors 39(4):415–421. <https://doi.org/10.1002/biof.1082>

49. Takahama U, Hirota S (2018) Interactions of flavonoids with α -amylase and starch slowing down its digestion. *Food Funct* 9(2):677–687. <https://doi.org/10.1039/C7FO01539A>
50. Trott O, Olson AJ (2010) AutoDock Vina: improving the speed and accuracy of docking with a new scoring function, efficient optimization, and multithreading. *J Comput Chem* 31(2):455–461. <https://doi.org/10.1002/jcc.21334>
51. Valenzuela-Atondo DA, Delgado-Vargas F, López-Angulo G, Calderón-Vázquez CL, Orozco-Cárdenas ML, Cruz-Mendivil A (2020) Antioxidant activity of *in vitro* plantlets and callus cultures of *Randia echinocarpa*, a medicinal plant from northwestern Mexico. *In Vitro Cell Dev Biol-Plant* 56:440–446. <https://doi.org/10.1007/s11627-020-10062-3>
52. Valitova JN, Sulkarnayeva AG, Minibayeva FV (2016) Plant sterols: diversity, biosynthesis, and physiological functions. *Biochem Mosc* 81:819–834. <https://doi.org/10.1134/S0006297916080046>
53. Villaseñor JL (2016) Checklist of the native vascular plants of Mexico. *Revista Mexicana de Biodiversidad* 87(3):559–902. <https://doi.org/10.1016/j.rmb.2016.06.017>
54. Wang J, Yuan B, Huang B (2019) Differential heat-induced changes in phenolic acids associated with genotypic variations in heat tolerance for hard fescue. *Crop Sci* 59(2):667–674. <https://doi.org/10.2135/cropsci2018.01.0063>
55. Wei Z, Li J (2020) Regulation of brassinosteroid homeostasis in higher plants. *Front Plant Sci* 11:583622. <https://doi.org/10.3389/fpls.2020.583622>
56. Xia J, Wishart DS (2016) Using MetaboAnalyst 3.0 for comprehensive metabolomics data analysis. *Curr Protoc Bioinformatics* 55(1):14–10. <https://doi.org/10.1002/cpbi.11>
57. Xu JJ, Fang X, Li CY, Yang L, Chen XY (2020) General and specialized tyrosine metabolism pathways in plants. *Abiotech* 1:97–105. <https://doi.org/10.1007/s42994-019-00006-w>
58. Yañez-Apam J, Herrera-González A, Domínguez-Uscanga A, Guerrero-Analco JA, Monribot-Villanueva JL, Fragoso-Medina JA, Luna-Vital DA (2023) Effect of the enzymatic treatment of phenolic-rich pigments from purple corn (*Zea mays* L.): Evaluation of thermal stability and alpha-glucosidase inhibition. *Food Bioprocess Technol* 16:1–15. <https://doi.org/10.1007/s11947-023-03021-4>

Figures

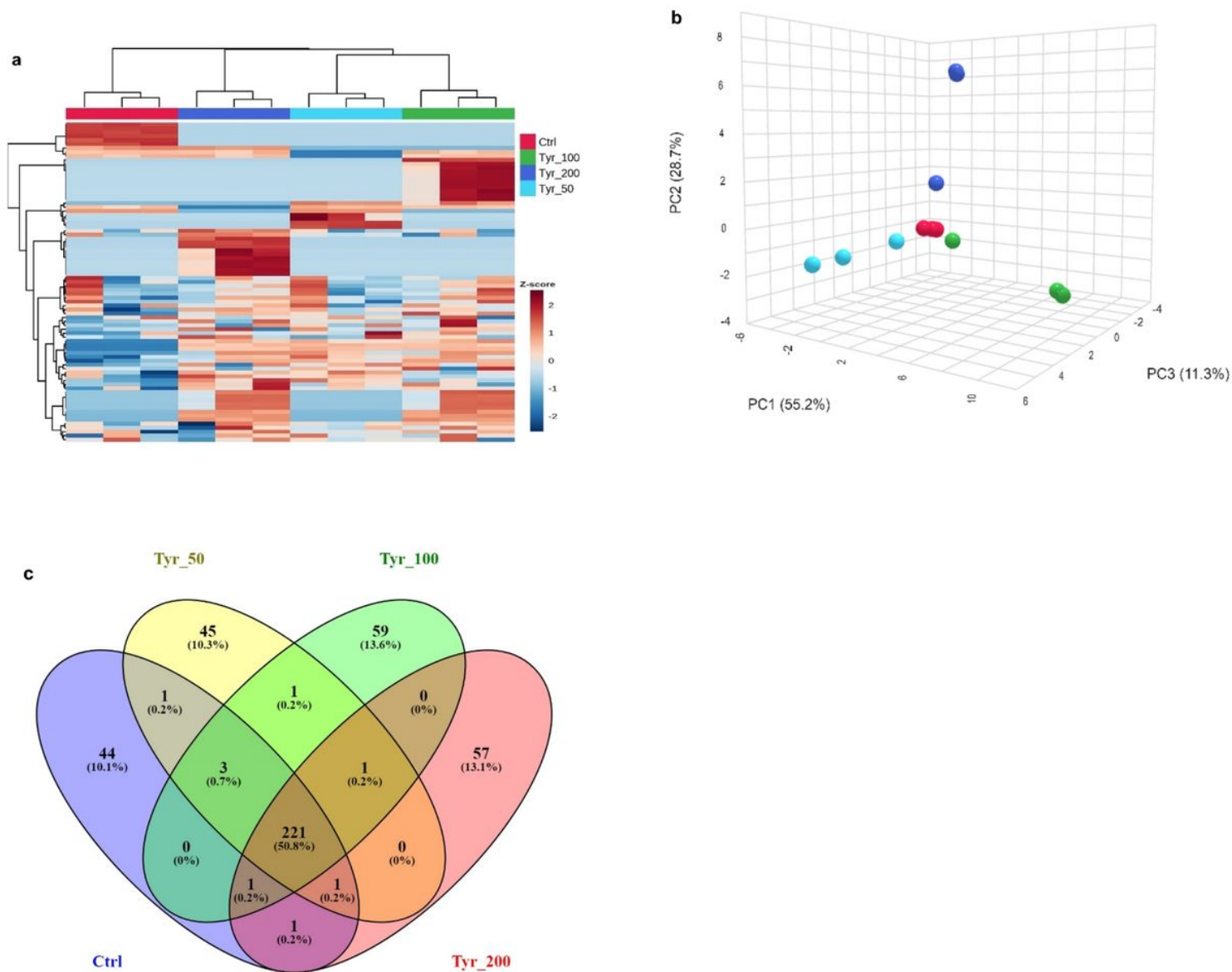


Figure 1

Untargeted metabolomic analysis of *R. echinocarpa* cell suspensions treated with different concentrations of Tyr. a) Heatmap with hierarchical clustering (HCA) showing the intensity of each Rt-m/z signal indicated by the z-score using a red (increased) and blue (decreased) scale. b) Principal component analysis (PCA) of Rt-m/z signals that changed due to the addition of 50 (sky blue), 100 (green) or 200 mg/L (dark blue) of tyrosine to the *R. echinocarpa* cell suspensions compared to control (red). c) Venn diagram showing the number of statistically significant Rt-m/z signals shared among Tyr treatments and control.

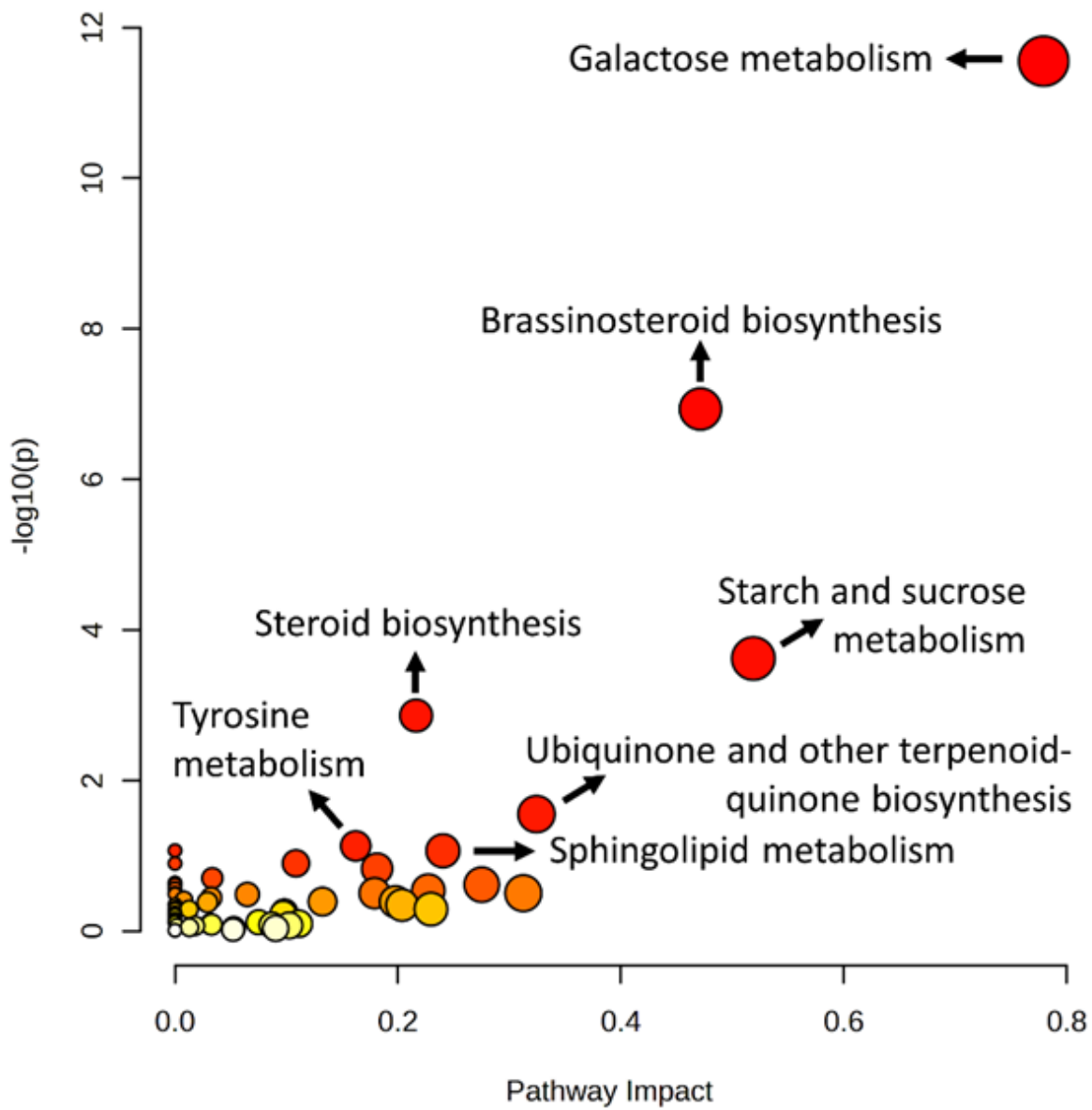


Figure 2

Functional analysis considering all the signals detected by the metabolomic analysis. Big red circles are related to the pathways with higher $-\log_{10}(p\text{-value})$ and impact, followed by smaller red, orange, and yellow circles.

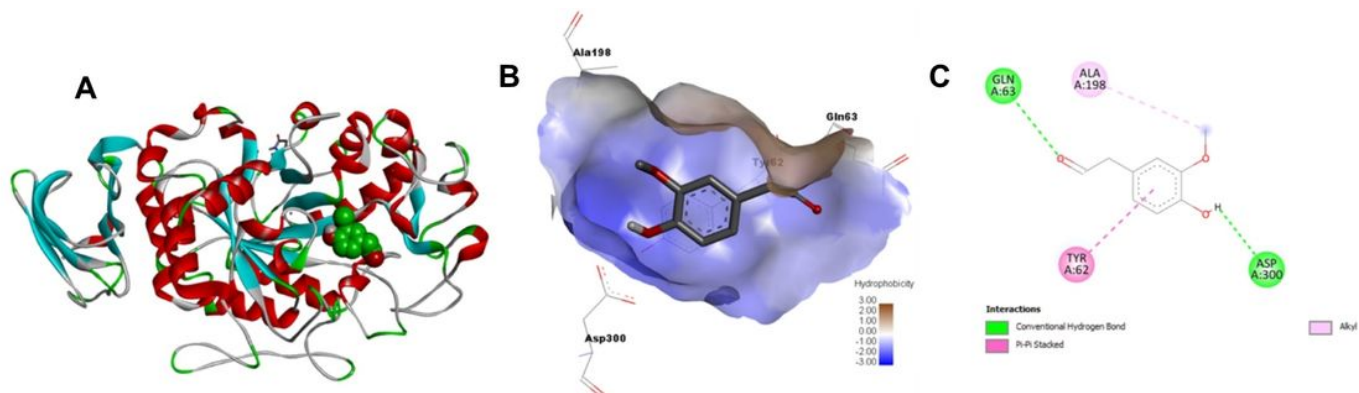


Figure 3

Molecular docking diagrams exemplifying the analysis of the best pose within the catalytic site of homovanillic acid 4-glucuronide (A). Additionally, their respective pose in the catalytic site depicting the hydrophobic environment is shown (B). 2D interacting diagrams are shown for homovanillic acid 4-glucuronide (C).